Supporting Information

Precision Therapy through Breaking the Intracellular Redox Balance with MOFs-based Intelligent Hydrogel Nanobot for Enhancing Ferroptosis and Activating Immunotherapy

Dongsheng Zhang,[a†] Yanfei Meng, [a,b†] Yingzi Song, [a,b] Ping Cui, [*a,b] Zunfu Hu, [*a,c] and Xiuwen Zheng[*a,b]

a. Key Laboratory of Functional Nanomaterials and Technology in Universities of Shandong, Linyi University, Linyi 276000, Shandong, P.R. China.

b. College of Chemistry & Chemical Engineering, Linyi University, Linyi 276000, Shandong, P.R. China.

c. School of Material Science and Engineering, Linyi University, Linyi 276000, Shandong, P.R. China.

† These authors contributed equally to this work.

* E-mail: zhengxiuwen@lyu.edu.cn.

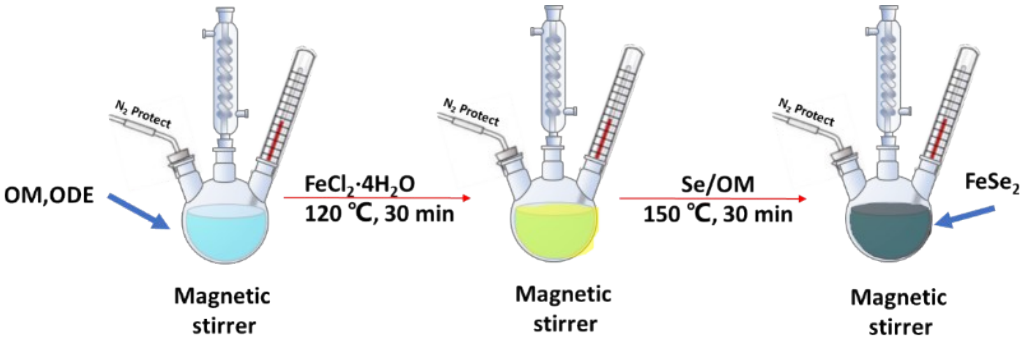

Fig. S1 Schematic representation for the preparation of $FeSe_2$ NPs.

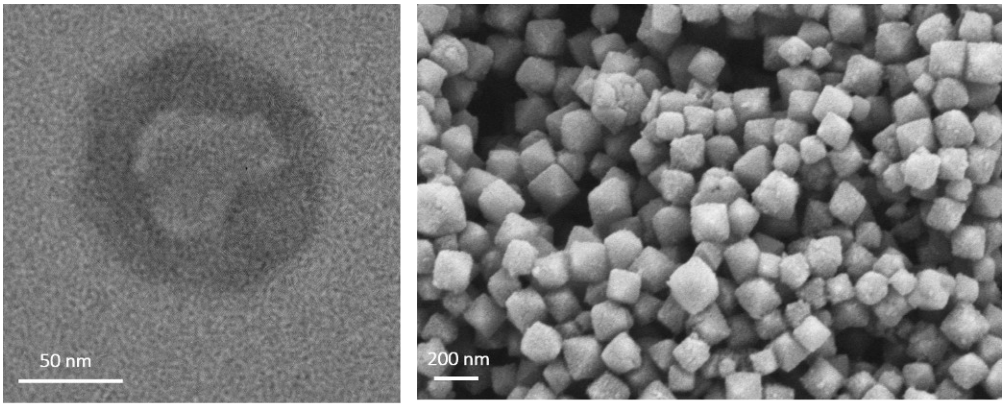

Fig. S2 (a) TEM image of HA/PEI/CpG NCs. (b) SEM image of FSMH nanohydrogel.

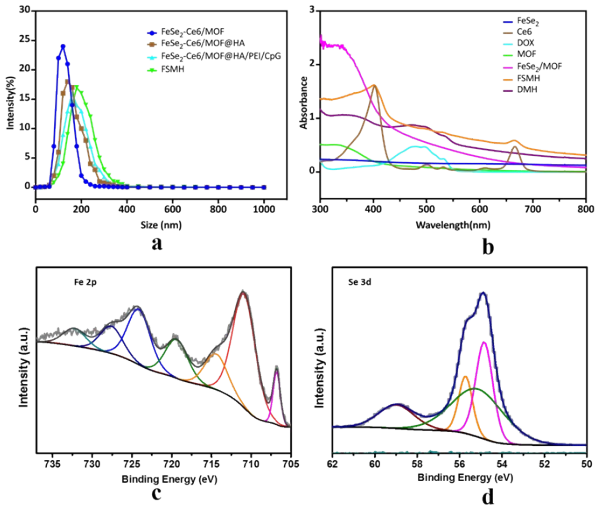

Fig. S3 (a) Size distribution of $FeSe_2$-Ce6/MOF NCs, $FeSe_2$-Ce6/MOF@HA NCs, $FeSe_2$-Ce6/MOF@HA/PEI/CpG NCs, and FSMH nanohydrogel from DLS analysis. (b) UV-vis spectra of the as-synthesized FSMH nanohydrogel, DMH, $FeSe_2$/MOF, MOF, $FeSe_2$, free Ce6 and free DOX. (c-d) The XPS spectra of $FeSe_2$ NPs, including Fe 2p (c) and Se 3d (d).

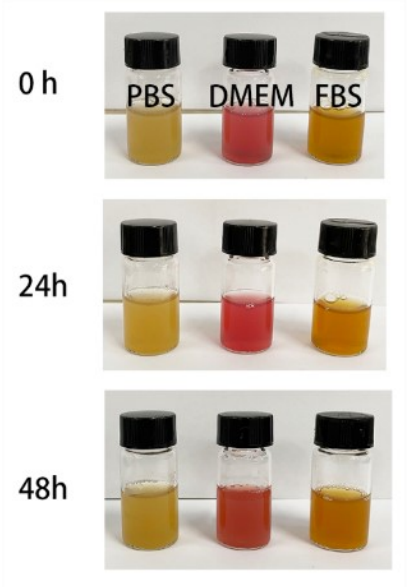

Fig. S4 Stability characterization of the FSMH nanohydrogel dispersed in PBS, FBS, and DMEM medium, respectively.

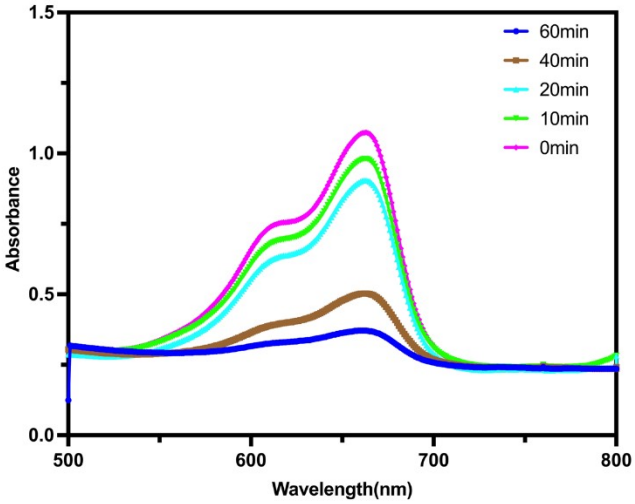

Fig. S5 UV–vis spectra of MB after degradation in a different time.

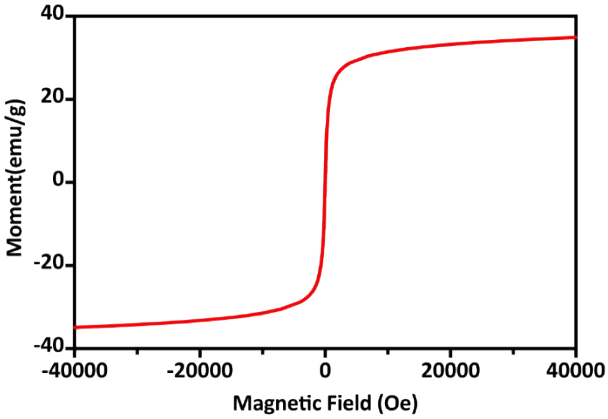

Fig. S6 The magnetic hystersis loop of $FeSe_2$ NPs at room temperature (298K).

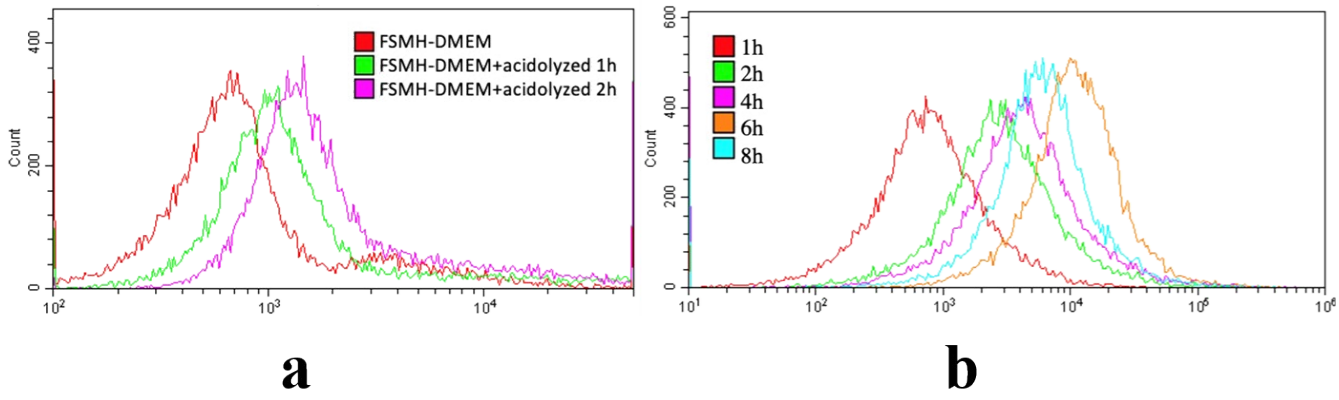

a **b**

Fig. S7 (a) Flow cytometric analysis of cell uptake of different environment in vitro. (b) Flow cytometric analysis of cell uptake of different time in vitro.

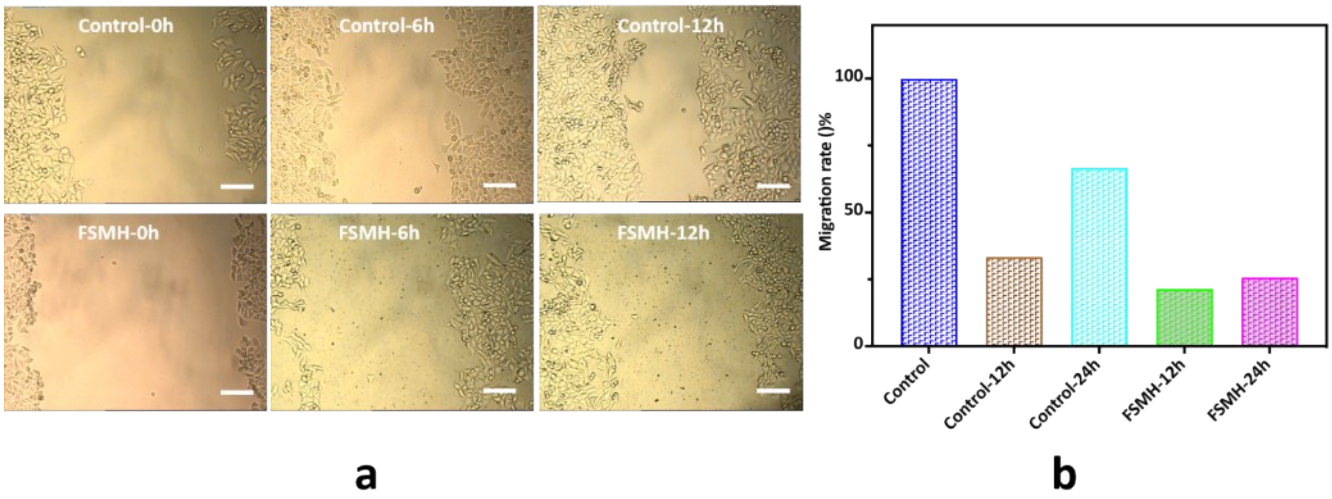

Fig. S8 (a) Inhibitory effects of FSMH nanohydrogel on 4T1 cell migration. Scale car: 100 μm. (b) Migration rate of 4T1 cells after treatment with FSMH nanohydrogel system.

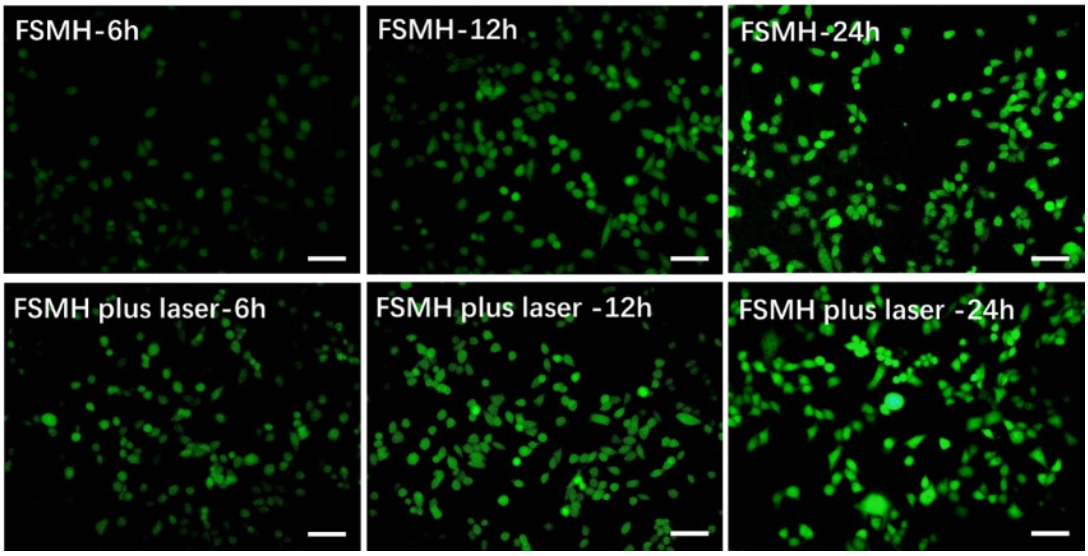

Fig. S9 ROS staining in 4T1 cells with indicated treatments different time. Scale car: 100 μm.

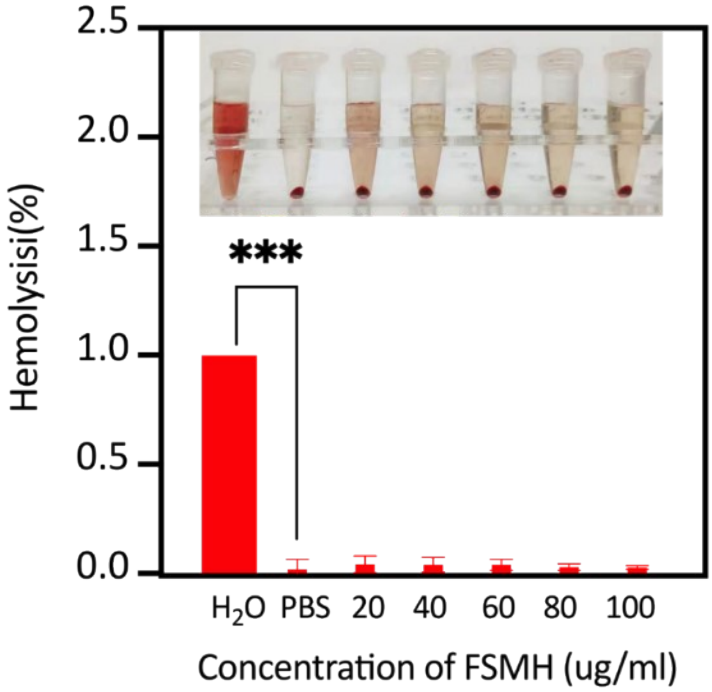

Fig. S10 Corresponding hemolysis rates of the RBC. The inset shows the photograph of RBC suspensions after treatment with various concentrations of FSMH. (***$p < 0.001$)

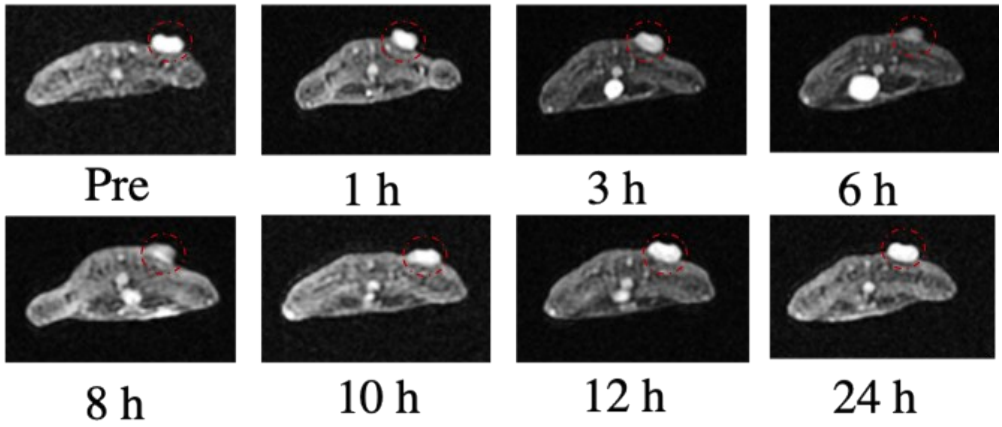

Fig. S11 In vivo T_2-weighted MR imaging of a 4T1 tumor-bearing mouse at different time intervals after intratumor injection with FMSH nanohydrogel system.

Fig. S12 Representative digital photos of 4T1-tumor-bearing mice after different treatments.

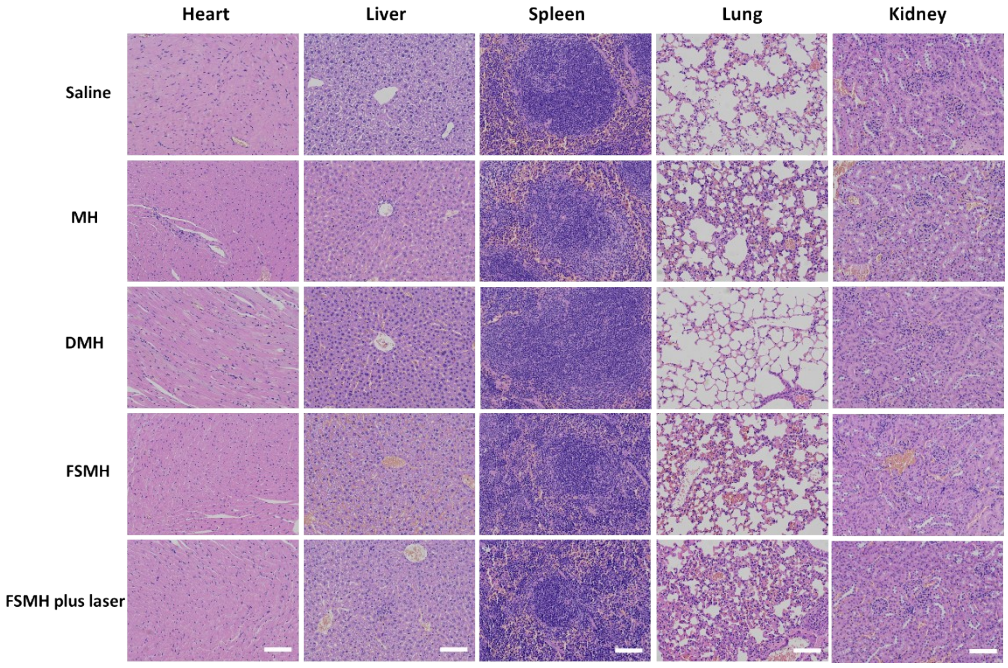

Fig. S13 H&E staining images of dissected major organs (heart, liver, spleen, lung, kidney) of 4T1 tumor-bearing mice after various treatments by intravenous administration. Scale bar: 100 μm.

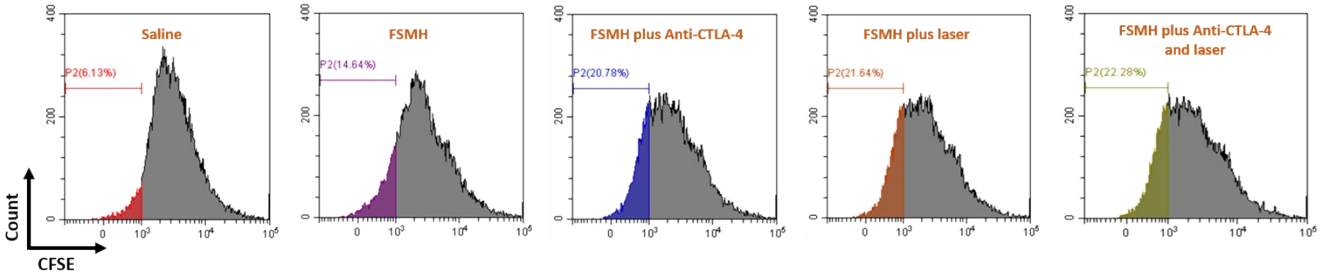

Fig. S14 Flow cytometry results of T cell proliferation in Peripheral blood lymphocytes of mice with different treated 4T1 cells.

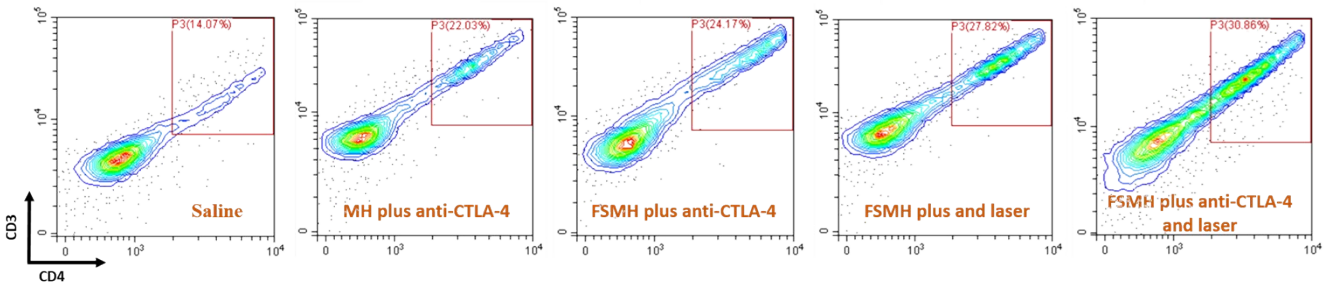

Fig. S15 Flow cytometric analysis of CTLs (CD3+CD4+ T cells) in the distant tumors in 4T1 tumor-bearing mice with different treatments.

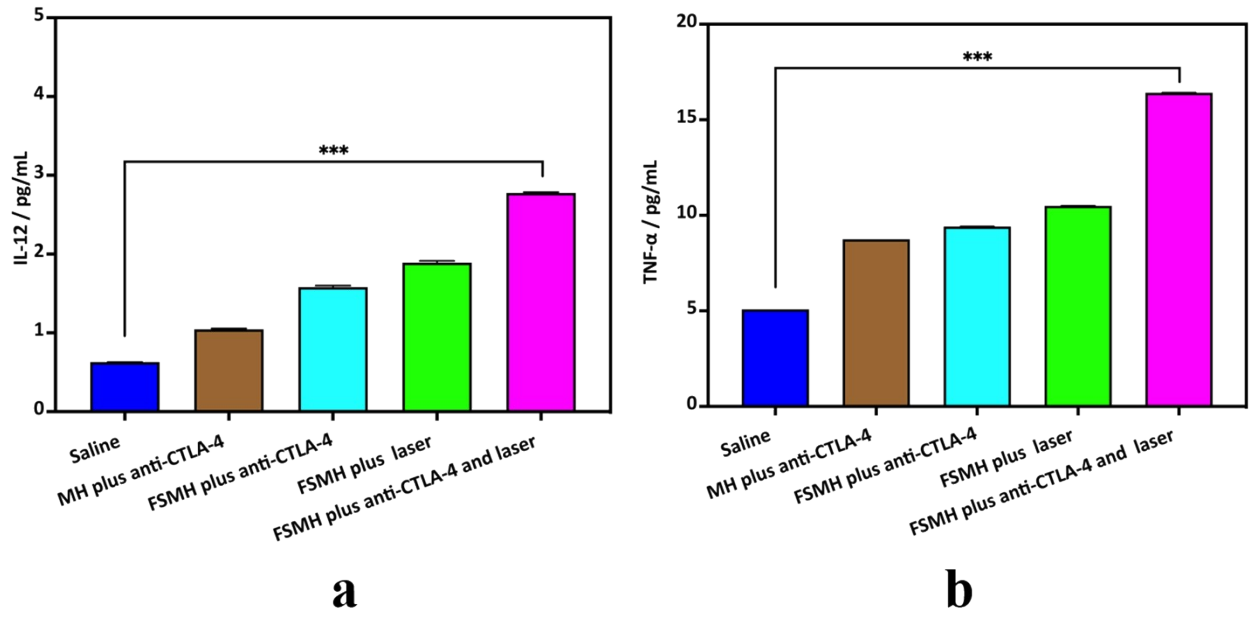

Fig S16: The secretion level of (c) IL-12 and (d) TNF-α by splenocytes obtained from immunized mice.